



Original Article

Effect of Sr and Y on microstructure and electrical conductivity of BaCeO₃

Siriwan Chokkha* and Sutin Kuharuangrong

*School of Ceramic Engineering,
Suranaree University of Technology, Mueang, Nakhon Ratchasima, 30000 Thailand.*

Received 21 March 2012; Accepted 1 July 2013

Abstract

The compositions of Sr doped BaCeO₃ synthesized by citrate gel method have been investigated as a potential proton conducting electrolyte for intermediate temperature solid oxide fuel cell (IT-SOFC). The average grain size of Ba_{0.9}Sr_{0.1}CeO₃ after sintering at 1,300°C decreased as compared to base material, however it increased with the amount of Sr. The highest grain conductivity is obtained from Ba_{0.9}Sr_{0.1}CeO₃ and its value at 700°C is 8.86×10⁻⁴ S.cm⁻¹. In addition, Y dopant was selected to further improve the electrical conductivity of Ba_{0.9}Sr_{0.1}CeO₃. The grain boundary conductivity at 700°C of Ba_{0.9}Sr_{0.1}Ce_{0.9}Y_{0.1}O_{3-δ} is 9.34×10⁻³ S.cm⁻¹.

Keywords: impedance spectra, conductivity, citrate gel, BaCeO₃

1. Introduction

Solid oxide fuel cell (SOFC) electrolyte based on yttria stabilized zirconia (YSZ) is required to operate at high temperature above 850°C to maintain the ionic conductivity (Lee *et al.*, 2003). A high operating temperature has many problems such as high cost, limit of materials for the unit cell components, thermal expansion mismatch and others. To solve these problems, many researchers have developed new electrolyte materials to reduce the operating temperature down to 500–650°C. The candidate materials such as ceria (Wang *et al.*, 2006), lanthanum gallate, barium cerate (Lin *et al.*, 2007; Chiodelli *et al.*, 2009) and other electrolyte materials have been extensively investigated to replace YSZ. For ceria, Gd and Sm dopants gave high ionic conductivity. However, doped ceria is required to sinter at high temperature to achieve high density electrolyte. In addition, it shows electronic conductivity at low oxygen partial pressures due to the reduction of Ce⁴⁺ to Ce³⁺. For lanthanum gallate, strontium and magnesium dopants increase its ionic conduc-

tivity but encounter the chemical instability with electrode materials (Fergus *et al.*, 2006; Li *et al.*, 2010). BaCeO₃ has been considered as a candidate for high proton conducting electrolyte operating at 400–700°C. There are many research works on BaCeO₃ with the dopants on B-site such as Y, Zr, Ti, Nb, Sm, Nd, Dy and Gd (Su *et al.*, 2006; Liou *et al.*, 2008; Zunic *et al.*, 2009). The grain conductivity at 600°C of BaCeO₃ synthesized by solid state method is 3×10⁻⁷ S.cm⁻¹ (Loridant *et al.*, 1995). For Nd doped BaCeO₃, the value of grain conductivity at 500°C is between 1.78–2.26×10⁻⁴ S.cm⁻¹ depending upon the preparation methods (Su *et al.*, 2006). The conductivity of Nb and Sm co-doped BaCeO₃ is 2.26×10⁻³ S.cm⁻¹ at 700°C (Xie *et al.*, 2009). With 10 mol% of Y dopant, the conductivity of BaCeO₃ is 9.6×10⁻⁴ S.cm⁻¹ at 700°C and 3.1×10⁻⁴ S.cm⁻¹ at 500°C (Matsumoto *et al.*, 2008). Only a few works have been published on A-site dopant, such as Sr and K (Yan *et al.*, 2009). The conductivity of Ba_{0.9}Sr_{0.1}Ce_{0.8}Y_{0.2}O_{3-δ} prepared by conventional solid state and sintered at 1,600 °C is 2.3×10⁻² S.cm⁻¹ at 750°C (Hung *et al.*, 2009).

In this work, the compositions of Ba_{1-x}Sr_xCeO₃ (x = 0-0.3) were synthesized by citrate gel method. The phase, microstructure and electrical conductivity of all compositions have been investigated using X-ray diffractometer

*Corresponding author.

Email address: meinoi_ceramic@hotmail.com

(XRD), scanning electron microscope (SEM) and solartron impedance analyzer, respectively. To further improve the electrical conductivity, Y is selected as co-dopant with Sr of $\text{Ba}_{1-x}\text{Sr}_x\text{CeO}_3$ compositions, which exhibit highest conductivity.

2. Materials and Experimental Procedures

Sr and Y doped BaCeO_3 were synthesized by citrate gel method. The starting materials using $\text{Ba}(\text{NO}_3)_2$ (99.5% purity), $\text{Ce}(\text{NO}_3)_3 \cdot 6\text{H}_2\text{O}$ (99% purity), citric acid and other doped materials, such as $\text{Sr}(\text{NO}_3)_2$ (99.5% purity) and $\text{Y}(\text{NO}_3)_3 \cdot 6\text{H}_2\text{O}$ (99.9% purity), were dissolved in deionized water. After mixing with a magnetic stirrer, nitric acid was added to complete dissolution and followed by citric acid as the polymerizable combustion fuel. The mole ratio of the metal ions and citric acid was 1:2. The mixed solution was introduced and heated on a hot plate. After the water evaporated, the solution became viscous and changed to yellow gel. During continuous heating, the auto-combustion started at 110°C until the reaction completed and appeared to be dark gray residues.

After grinding, the residue powders were calcined in air and held at the reaction temperatures determined from differential thermal analyzer (DTA) using the temperature range from room temperature to $1,200^\circ\text{C}$ in air with a heating rate of $10^\circ\text{C}/\text{min}$. The room temperature phase of calcined powder was investigated by means of X-ray diffraction using Bruker D5005 with $\text{Cu K}\alpha$ in the 2-theta range of 20° - 90° . The disk specimens were formed by cold-isostatic press at 150 MPa and sintered at $1,300^\circ\text{C}$ for 2 hrs in air.

The microstructure of sintered specimens was observed by scanning electron microscope (SEM, Jeol JSM6400). The samples were polished and thermally etched before gold sputtering. The AC impedance spectra of sintered compositions were collected from 300°C to 800°C by a Solartron impedance analyzer (SI 1260A) as a function of frequency. All data were measured in air and sample temperatures were recorded with a thermocouple type K mounted close to the sample.

3. Results and Discussion

The DTA result of Sr doped BaCeO_3 after synthesized by citrate gel method shows in Figure 1. The reactions occur as indicated by the arrows at 280°C , 580°C , 810°C and 900°C , respectively. Although the reactions complete at 900°C , the actual calcination temperature at 950°C with a soaking period for 4 hrs is employed for a large amount of powder to obtain a single phase for all compositions.

Figure 2 shows the results of XRD for $\text{Ba}_{1-x}\text{Sr}_x\text{CeO}_3$ ($x = 0-0.3$) powder after calcination at 950°C for 4 hrs in air. All compositions show a single phase in agreement with JCPDS No. 82-2425. With an increasing amount of Sr dopant, the peaks shift to higher two-theta angles, indicating a decrease of the lattice parameter. This is due to the partial

substitution of smaller ionic radius of Sr for Ba.

The SEM micrographs of $\text{Ba}_{1-x}\text{Sr}_x\text{CeO}_3$ ($x = 0-0.3$) sintered at $1,300^\circ\text{C}$ for 2 hrs show in the Figure 3a-d. The average grain size of BaCeO_3 is 4-5 μm (Figure 3a) which is higher than that of $\text{Ba}_{0.9}\text{Sr}_{0.1}\text{CeO}_3$ (Figure 3b). Addition of Sr with $x = 0.1$ not only decreases the average grain size but increases the density of BaCeO_3 . However, further increasing amount of Sr tends to increase the average grain size and porosity as shown in Figure 3c-d. Therefore, an increasing amount of Sr decreases the density of BaCeO_3 .

The impedance spectra measured in air at 400°C for undoped and Sr doped BaCeO_3 are shown in Figure 4. The results of two arcs for $\text{Ba}_{1-x}\text{Sr}_x\text{CeO}_3$ ($x = 0$ and 0.1) respond to the contributions from grain and grain boundaries. They are associated with the capacitances in the pF and nF ranges, respectively. However, the impedance of grain boundaries for the compositions of $x = 0.2-0.3$ cannot be obtained due to the limited frequency of equipment. $\text{Ba}_{0.9}\text{Sr}_{0.1}\text{CeO}_3$ shows the lowest resistance for both of grain interior and grain bound-

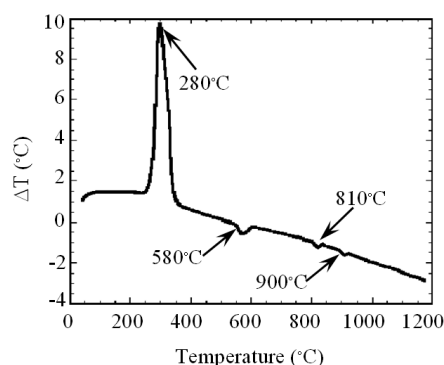


Figure 1. DTA of Sr doped BaCeO_3 residue composition.

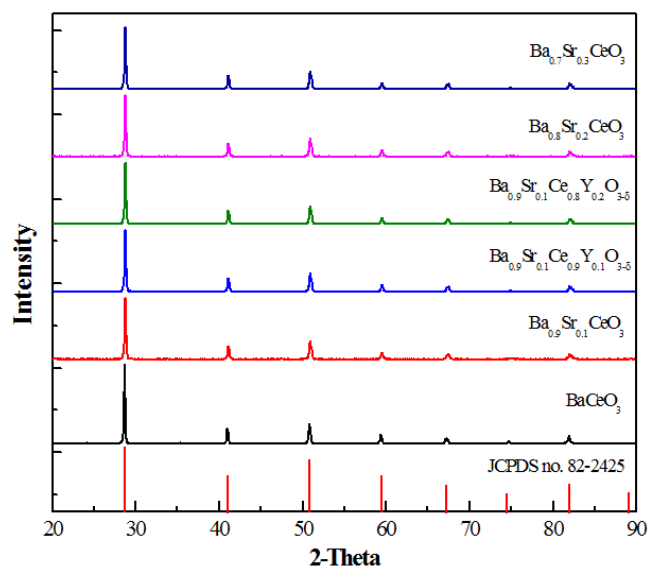


Figure 2. XRD patterns of calcined powders prepared by citrate gel method.

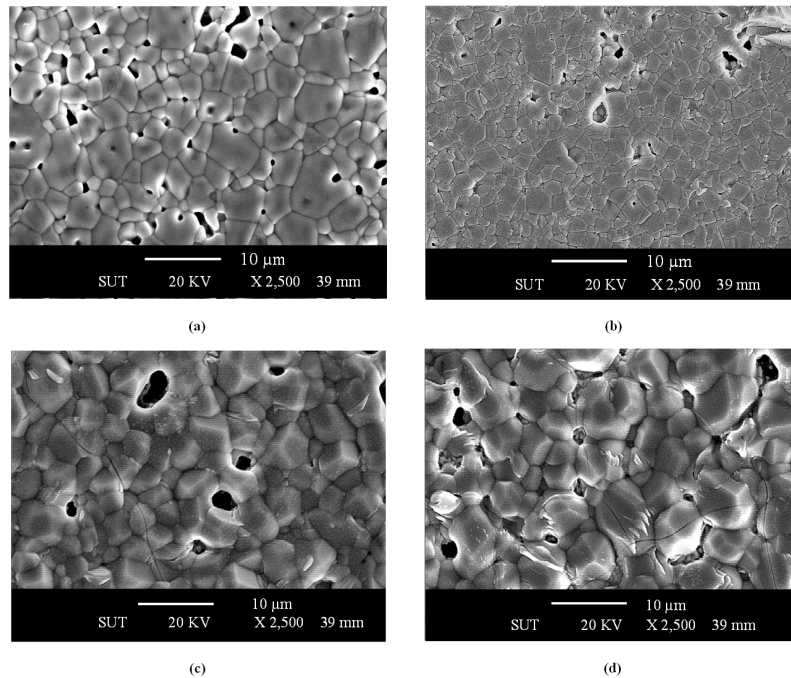


Figure 3. SEM micrographs of sintered compositions (a) BaCeO_3 , (b) $\text{Ba}_{0.9}\text{Sr}_{0.1}\text{CeO}_3$, (c) $\text{Ba}_{0.8}\text{Sr}_{0.2}\text{CeO}_3$ and (d) $\text{Ba}_{0.7}\text{Sr}_{0.3}\text{CeO}_3$.

ary determined from the width of each arc as compared to other compositions. This is possibly due to smaller grains and lower number of pores obtained for this composition. An increasing amount of Sr dopant tends to increase the grain resistance and $x = 0.3$ shows the highest grain resistance of this study. These results indicate that the grain size and porosity affect the conductivity of BaCeO_3 .

Arrhenius plots of grain conductivities for all compositions are shown in Figure 5. The grain conductivity of $\text{Ba}_{0.9}\text{Sr}_{0.1}\text{CeO}_3$ is higher than that of the other compositions for all measured temperatures and the lowest conductivity occurs in $\text{Ba}_{0.7}\text{Sr}_{0.3}\text{CeO}_3$. The conductivity value of $\text{Ba}_{0.9}\text{Sr}_{0.1}\text{CeO}_3$ at 700°C is $8.86 \times 10^{-4} \text{ S}\cdot\text{cm}^{-1}$.

In order to improve the electrical conductivity of $\text{Ba}_{0.9}\text{Sr}_{0.1}\text{CeO}_3$, Y dopant was selected as co-dopant in $\text{Ba}_{0.9}\text{Sr}_{0.1}\text{Ce}_{1-y}\text{Y}_y\text{O}_{3-\delta}$ ($y = 0-0.2$). The single phase of Y dopant for these two compositions can be achieved as shown from XRD results in Figure 2. The impedance spectra results of Y dopant decrease the grain boundary resistivity of $\text{Ba}_{0.9}\text{Sr}_{0.1}\text{CeO}_3$ as shown in Figures 6 and 7. In addition, $y = 0.1$ shows the lowest resistance of grain boundaries as compared to the all compositions. However, an increasing amount of Y to $y = 0.2$ increases the grain boundary resistivity.

Figure 8 shows the Arrhenius plots of conductivities for $\text{Ba}_{0.9}\text{Sr}_{0.1}\text{Ce}_{1-y}\text{Y}_y\text{O}_{3-\delta}$ ($y = 0-0.2$). Grain boundary conductivity of $\text{Ba}_{0.9}\text{Sr}_{0.1}\text{Ce}_{0.9}\text{Y}_{0.1}\text{O}_{3-\delta}$ is higher than that of $\text{Ba}_{0.9}\text{Sr}_{0.1}\text{CeO}_3$ and $\text{Ba}_{0.9}\text{Sr}_{0.1}\text{Ce}_{0.8}\text{Y}_{0.2}\text{O}_{3-\delta}$ at all measurement temperatures. The SEM in Figure 9 exhibits uniform and small grain sizes of Y doped $\text{Ba}_{0.9}\text{Sr}_{0.1}\text{CeO}_3$ resulting in a

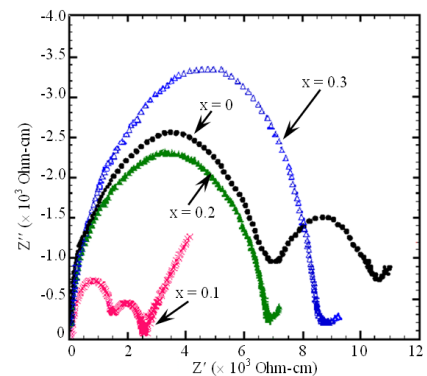


Figure 4. Impedance spectra at 400°C for $\text{Ba}_{1-x}\text{Sr}_x\text{CeO}_3$.

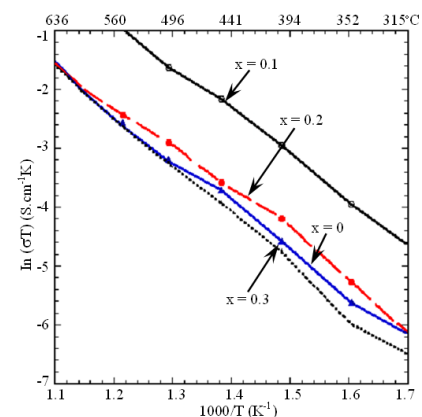


Figure 5. Arrhenius plots of conductivity for $\text{Ba}_{1-x}\text{Sr}_x\text{CeO}_3$.

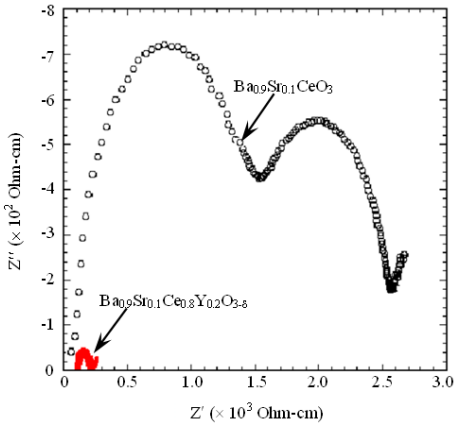


Figure 6. Impedance spectra at 400°C for $Ba_{0.9}Sr_{0.1}CeO_3$ and $Ba_{0.9}Sr_{0.1}Ce_{0.8}Y_{0.2}O_{3-\delta}$.

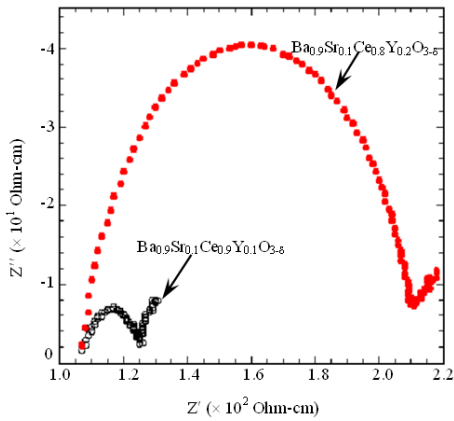


Figure 7. Impedance spectra at 400°C for $Ba_{0.9}Sr_{0.1}Ce_{0.9}Y_{0.1}O_{3-\delta}$ and $Ba_{0.9}Sr_{0.1}Ce_{0.8}Y_{0.2}O_{3-\delta}$.

lower resistance of this composition. The grain boundary conductivity value of $Ba_{0.9}Sr_{0.1}Ce_{0.9}Y_{0.1}O_{3-\delta}$ at 700 °C is $9.34 \times 10^{-3} S.cm^{-1}$. The conductivity increases as the temperature increases and its values at 500, 600, and 700°C including activation energies determined from the slope of the plot for all compositions are given in Table 1.

4. Conclusions

The single phase of $Ba_{1-x}Sr_xCeO_3$ ($x = 0-0.3$) synthesized by citrate gel method can be obtained after calcination at 950°C for 4 hrs in air. The average grain size and porosity of $Ba_{0.9}Sr_{0.1}CeO_3$ are lower than those of other compositions after sintering at 1,300°C for 2 hrs. In addition, $Ba_{0.9}Sr_{0.1}CeO_3$ shows the highest total conductivity as compared to the other compositions at all measuring temperatures. The conductivity of $Ba_{0.9}Sr_{0.1}CeO_3$ at 700°C is $8.86 \times 10^{-4} S.cm^{-1}$. Y as co-dopant, $Ba_{0.9}Sr_{0.1}Ce_{0.9}Y_{0.1}O_{3-\delta}$ exhibits the highest grain boundary conductivity at low sintered temperature of 1,300°C and its conductivity value at 700°C is $9.34 \times 10^{-3} S.cm^{-1}$.

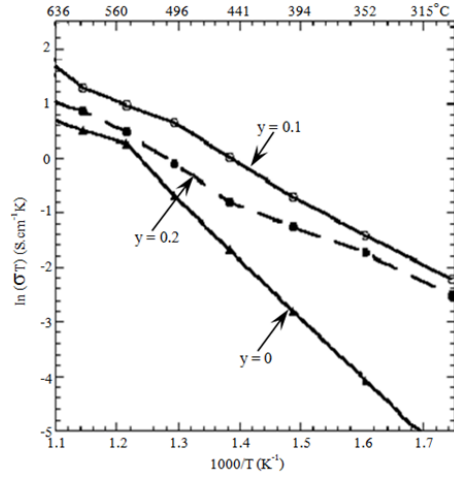
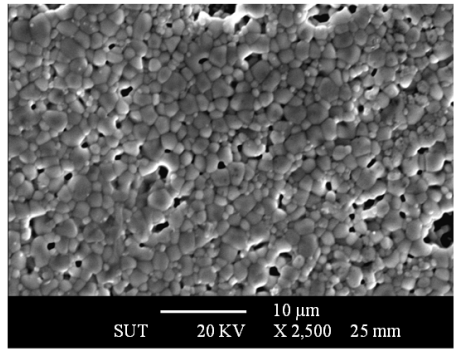
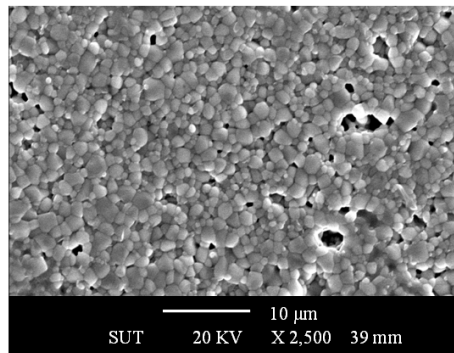


Figure 8. Arrhenius plots of grain boundary conductivity for $Ba_{0.9}Sr_{0.1}Ce_{1-y}Y_yO_{3-\delta}$ ($y = 0-0.2$).



(a)



(b)

Figure 9. SEM micrographs of sintered compositions (a) $Ba_{0.9}Sr_{0.1}Ce_{0.9}Y_{0.1}O_{3-\delta}$ and (b) $Ba_{0.9}Sr_{0.1}Ce_{0.8}Y_{0.2}O_{3-\delta}$.

Acknowledgements

This work was supported by the National Science and Technology Development Agency (University-Industry Research Collaboration; U-IRC).

Table 1. Grain boundary conductivity of $\text{Ba}_{1-x}\text{Sr}_x\text{Ce}_{1-y}\text{Y}_y\text{O}_{3-\delta}$ and the activation energies.

Compositions	σ (S.cm^{-1})	σ (S.cm^{-1})	σ (S.cm^{-1})	E_a (eV)
	T = 500 °C	T = 600 °C	T = 700 °C	
x = 0, y = 0	5.13×10^{-5}	1.13×10^{-4}	2.29×10^{-4}	0.70
x = 0.1, y = 0	2.55×10^{-4}	6.28×10^{-4}	8.86×10^{-4}	0.61
x = 0.2, y = 0	5.12×10^{-5}	1.55×10^{-4}	4.05×10^{-4}	0.69
x = 0.3, y = 0	4.97×10^{-5}	1.53×10^{-4}	3.89×10^{-4}	0.73
x = 0.1, y = 0.1	2.48×10^{-3}	4.19×10^{-3}	9.34×10^{-3}	0.54
x = 0.1, y = 0.2	1.17×10^{-3}	2.75×10^{-3}	5.25×10^{-3}	0.52

References

- Chiodelli, G., Malavasi, L., Tealdi, C., Barison, S., Battagliarin, M., Doubova, L., Fabrizio, M., Mortalò, C. and Gerbasi, R. 2009. Role of synthetic route on the transport properties of $\text{BaCe}_{1-x}\text{Y}_x\text{O}_3$ proton conductor. *Journal of Alloys Compounds*. 470(1-2), 477-485.
- Fergus, J.W. 2006. Electrolytes for solid oxide fuel cells. *Journal of Power Sources*. 162(1), 30-40.
- Hung, I.M., Peng, H.W., Zheng, S.L., Lin, C.P. and Wu, J.S. 2009. Phase stability and conductivity of $\text{Ba}_{1-y}\text{Sr}_y\text{Ce}_{1-x}\text{Y}_x\text{O}_{3-\delta}$ solid oxide fuel cell electrolyte. *Journal of Power Sources*. 193(1), 155-159.
- Lee, D.W., Won, J.H. and Shim, K.B. 2003. Low temperature synthesis of BaCeO_3 nano powders by the citrate process. *Materials Letters*. 57(22-23), 3346-3351.
- Li, S., Li, Z. and Bergman, B. 2010. Lanthanum gallate and ceria composite as electrolyte for solid oxide fuel cells. *Journal of Alloys Compounds*. 492(1-2), 392-395.
- Liou, Y.C. and Yang, S.L. 2008. A simple and effective process for $\text{Sr}_{0.995}\text{Ce}_{0.95}\text{Y}_{0.05}\text{O}_{3-\delta}$ and $\text{BaCe}_{0.9}\text{Nd}_{0.1}\text{O}_{3-\delta}$ solid electrolyte ceramics. *Journal of Power Sources*. 179(2), 553-559.
- Lin, H.L., Chiang, R.K., Kuo, C.L. and Chang, C.W. 2007. Synthesis of BaCeO_3 powders by a fast aqueous citrate-nitrate process. *Journal of Non-Crystalline Solids*. 353(11-12), 1188-1194.
- Loridant, S., Abello, L., Siebert, E. and Lucazeau, G. 1995. Correlations between structural and electrical properties of BaCeO_3 studied by coupled in-situ Raman scattering and impedance spectroscopy. *Solid State Ionics*. 78(3-4), 249-258.
- Matsumoto, H., Nomura, I., Okada, S. and Ishihara, T. 2008. Intermediate-temperature solid oxide fuel cells using perovskite-type oxide based on barium cerate. *Solid State Ionics*. 179(27-32), 1486-1489.
- Su, X.T., Yan, Q.Z., Ma, X.H., Zhang, W.F. and Ge, C.C. 2006. Effect of co-dopant addition on the properties of yttrium and neodymium doped barium cerate electrolyte. *Solid State Ionics*. 177(11-12), 1041-1045.
- Wang, Y., Mori, T., Li, J.G., Yajima, Y. and Drennan, J. 2006. Synthesis, characterization and sinterability of 10 mol% Sm_2O_3 -doped CeO_2 nanopowders via carbonate precipitation. *Journal of the European Ceramic Society*. 26(4-5), 417-422.
- Yan, R., Chen, G., Wang, F., Wang, Q. and Huang, W. 2009. A novel proton conducting $\text{Ba}_{0.95}\text{K}_{0.05}\text{Ce}_{0.6}\text{Zr}_{0.2}\text{Gd}_{0.16}\text{Zn}_{0.04}\text{O}_3$ for SOFC. *Journal of Alloys Compounds*. 486(1-2), L10-L12.
- Xie, K., Yan, R., Chen, X., Dong, D., Wang, S., Liu, X. and Meng, G. 2009. A new stable BaCeO_3 -base proton conductor for intermediate-temperature solid oxide fuel cell. *Journal of Alloys Compounds*. 472(1-2), 551-555.
- Zunic, M., Chevallier, L., Deganello, F., D'Epifanio, A., Licoccia, S., Di Bartolomeo, E. and Traversa, E. 2009. Electrophoretic deposition of dense $\text{BaCe}_{0.9}\text{Y}_{0.1}\text{O}_{3-x}$ electrolyte thick-films on Ni-based anodes for intermediate temperature solid oxide fuel cells. *Journal of Power Sources*. 190(2), 417-422.